MODELING GROOVED ROLLS WITH MOVING 2D POROUS MEDIA

By

Simo Nurmi[1], Fredrik Berström[1], Eero Immonen[1], Antti Lehtinen[1], Kari Juppi[2], and Lars Martinsson[3]
[1]Process Flow Ltd Oy
[2]Metso Paper Oy
FINLAND
[3]Albany International AB
SWEDEN

ABSTRACT

Rolls are widely used in paper machines to heat, press and support paper webs and fabrics in order to facilitate rapid drying and transport of the paper web through the machine. In modern high speed paper machines, however, the interaction of boundary layer flows on the rolls, fabrics and the paper web often results in an undesirable pressure development at *nip* regions, ultimately causing an uncontrolled motion of the paper web. This *runnability* issue can be mitigated by using a so-called *suction roll* construction, which forces the required pressure profile over the paper web. Its operational costs are high, however. One result of the study is that the topology and the material of the roll surfaces, in particular the introduction of *grooves* on the smooth roll surfaces, can have a tremendous impact on the overall runnability potential of the paper web.

The complexity of solving the governing Navier-Stokes equations and the sheer variability of paper machine constructions makes a comprehensive *analytical* study of the roll-grooving effect difficult. To the authors' knowledge, analytical solutions for nip pressures only exist for two-dimensional geometries and for smooth roll's. Moreover, numerical 3D simulations of grooved rolls in large paper machine sections are not feasible with today's computational or modeling resources.

In this article, we propose a computational 2D model for a grooved roll. The model reproduces three-dimensional wall friction effects and minor losses in 2D by treating a grooved roll surface as a moving porous medium. The nip pressures are calculated and compared for:

a grooved roll interacting with a rigid impermeable horizontal wall at a tangent point (symmetric 3D)

a grooved roll interacting with a rigid impermeable horizontal wall at a tangent point where the groove geometry is described in 2D with moving porous media.

The roll models describe the roll as infinitely wide, thus capturing friction effects between the roll and the surrounding air. The simulations are conducted with the RANS-method of computational fluid dynamics (CFD) on a commercial solver.

The results show that the proposed computational 2D model for a grooved roll yields similar pressure profiles at nip regions as the more computationally expensive full-scale 3D models. The significance of this observation is that the 2D model now facilitates the study of grooved rolls in large sections of paper machines.

NOMENCLATURE

2D	2-dimensional
3D	3-dimensional
C	inertia loss term [kg/m^4]
C_2	pressure-jump coefficient [1/m]
D	viscous loss term [kg/m³s]
d	diameter [m]
f	friction factor [-]
G	groove fraction [-]
g	gravity [m/s²]
K	minor loss coefficient [-]
L	length [m]
m	thickness [m]
p	pressure [Pa]
Re	Reynolds number [-]
r	radius [m]
S	source term [N/m³]
s	roll tangential direction [m]
V	volume flow proportion [-]
$\dot{V}$	volume flow [m³/s]
v	velocity [m/s]
x	x-coordinate [m]
y	y-coordinate [m]
z	horizontal elevation [m]
α	angle [deg], permeability [m²]
β	angle [deg]
ρ	density [kg/m³]
μ	viscosity [kg/ms]

Superscripts

*	modified

Subscripts

	initial
	tangent point, radial component
2D	2-dimensional
a	atmospheric, air
e	emptying, entrainment, opening nip
eff	effective
exp	experimental
f	filling, fraction
g	groove
h	height, hydraulic
i	component

in	closing nip
l	roll land
lam	laminar
rad	radial
rel	relative
turb	turbulent
w	width
x	x-direction

INTRODUCTION

Web handling refers to controlling manufacturing processes where the main raw material is a continuous flexible membrane. Examples of industrial processes involving web handling include paper or plastic in the printing industry, cardboard in the packaging industry, rolled steel slabs of continuous steel in the steel industry, or magnetic tape in the recording industry. The membrane motion is significantly influenced by air flow motion, and hence, an understanding of fluid mechanics related to the transport of webs at high speed processes, such as drying, coating and calendering, and the fundamental principles of air movement near rolls and webs are of industrial interest.

Rolls are widely used in paper machines to heat, press and support paper webs and fabrics in order to facilitate rapid drying and transport of the paper web through the machine. In modern high speed paper machines, however, the interaction of boundary layer flows on the rolls, fabrics and paper web often results in an undesirable pressure development at *nip* regions, ultimately causing an uncontrolled motion of the paper web, i.e. runnability problems. The runnability problems might appear in modern single-run drying sections whereby the paper web is only supported on one of its sides by the dryer fabric. Figure 11 shows problematic areas in a single-run configuration with positive pressure (overpressure) and negative pressure (underpressure) caused by boundary layer flows on paper and fabric surfaces.

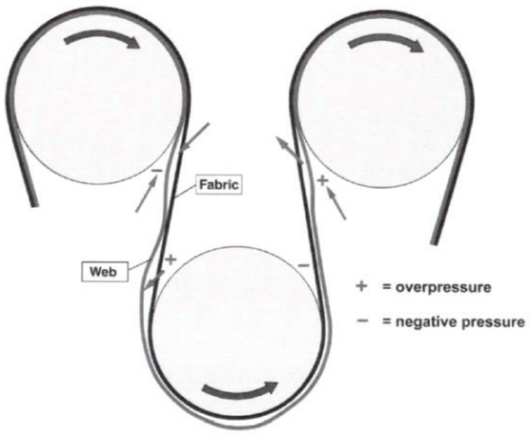

Figure 11 – Runnability problems in a dryer group [2].

The runnability issue can be mitigated by using a so-called *vacuum roll* construction and a *high velocity blow-box* [2]. The vacuum roll and blow-box force the required pressure profile over the paper web at the opening and closing nips of the drying section of the paper machine. The surface of the vacuum roll is often grooved, and the groove

bottoms are perforated. Suction through the roll removes the excess air from the closing nip, improving the runnability. A high velocity blow-box, on the other hand, increases the underpressure within the pocket area, keeping the paper attached to the fabric. A significant drawback of the vacuum roll construction is the high operational cost caused by the suction air through the vacuum roll. The need for energy efficiency raises the question of whether there is a way to improve the vacuum roll. This is the major theme of the present article.

A roll with large grooves has been introduced by Kurki and Martikainen in 2005 [3]. Their article presents insights into how roll grooves can yield an underpressure on the vacuum roll surface and thus improve the runnability in a single-run dryer group. Kurki and Martikainen [3] conducted measurements with a pilot paper machine and compared them with CFD calculations. One purpose of the circumferentially grooved rolls is to maintain traction between the rotating roll and the web. In the winding of the web, grooved rolls are used to prevent air bags in wound rolls [7]. A comparison of aerodynamic properties between a smooth and grooved roll can be found in Nurmi et al. [5]. The paper [5] also presents the basic aerodynamic functionality of the grooved roll as a function of groove dimensions, roll diameter and surface velocity. Their 3D model describes the flow conditions with infinitely wide roll construction capturing the groove friction effects and minor losses.

Numerical 3D simulations of grooved rolls in a large paper machine sections are not feasible with today's computational or modeling resources. In order to avoid detailed 3D modeling of the groove, a 2D model simplification with porous medium and porous jump boundary condition is needed. Such a 2D model would provide a means to study grooved rolls in large and complicated geometries based on actual paper machine sections.

In the present article, we propose a computational 2D model for a grooved roll. The model reproduces three-dimensional groove wall friction effects and minor losses in 2D by treating a grooved roll surface as a moving porous medium. The nip pressures are calculated and compared for a grooved roll interacting with a rigid impermeable horizontal wall at a tangent point (symmetric 3D) and for a grooved roll interacting with a rigid impermeable horizontal wall at a tangent point, where the groove geometry is described in 2D with the moving porous media. The closing and opening nip pressure of a grooved roll as a function of roll diameter, groove size and rotational speed is of interest and studied with the help of CFD-simulations. The simulations are based on Reynolds averaged Navier-Stokes solving methods performed with a commercial CFD-code, ANSYS Fluent.

MODEL DEVELOPMENT

3D Grooved Roll

The grooved roll CFD-model is a three-dimensional "*slice*", which consists of a half groove and a half of a roll land with symmetric boundary conditions. This simplification reduces the computational effort. The model describes the roll as infinitely wide, capturing entrance, exit, and friction effects between the groove and the surrounding air. The grooved roll configuration is presented in Figure 12.

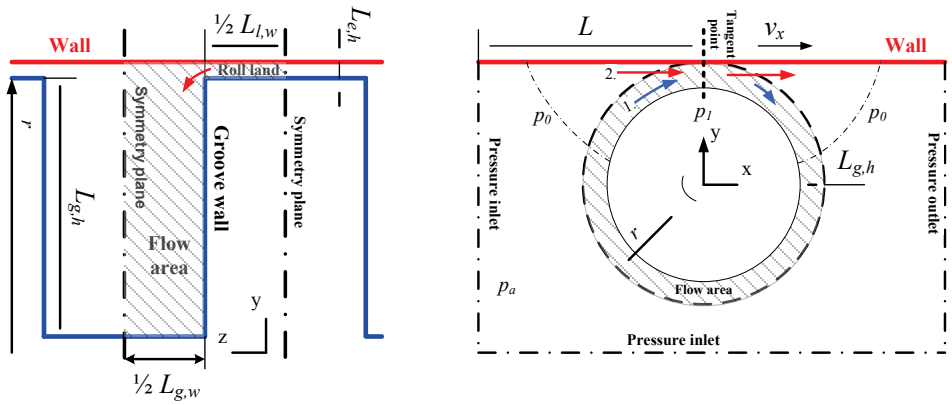

Figure 12 – 3-dimensional model for a grooved roll and the associated nomenclature and boundary conditions.

Basically air has two different routes to reach the tangent point: the first one (arrow 1, in Figure 12 and 3) is inside the roll groove. The second one (arrow 2, in Figure 12 and 3) is flow along the wall to the closing nip where flow bends to the groove. Depending on the wall velocities, the development length of the boundary layer and the groove geometry the air flow accelerates to a high speed at the tangent point. The air acceleration causes underpressure in the groove due to an increase of dynamic pressure. A challenge now arises: what are the flow losses in route 2? The flow experiences so called minor losses in the sudden contraction and flow direction change. At the same time, the friction losses in the groove and the diverging area between the wall and the groove land increase the flow losses. The assumption of frictionless flow cannot be made, and therefore the Bernoulli equation is not valid. In

Figure 13, we present a groove function principle considering the pressure losses.

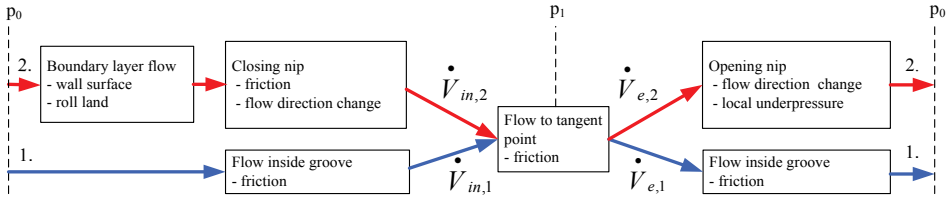

Figure 13 – Functionality of the 3D grooved roll model with nomenclature.

Subscript *in* stands for closing nip flow and *e* to opening nip flow. Subscript *1* stands for the flow inside of the groove and *2* to boundary layer flow along the wall surface. Since the flow solutions are strongly coupled, the volume flows are the same at the closing and opening nip. On the basis of the roll size, the groove geometry and boundary layer flows, the volume flow proportions change. On the closing nip side the groove filling fraction V_f is defined as

$$V_f = \frac{\dot{V}_{in,2}}{\dot{V}_{in,1} + \dot{V}_{in,2}} \qquad \{1\}$$

where $\dot{V}$ is volume flow. Similarly the groove emptying fraction V_e is

$$V_e = \frac{\dot{V}_{e,2}}{\dot{V}_{e,1} + \dot{V}_{e,2}} \quad \{2\}$$

The flow characteristic Reynolds number inside the groove is defined as

$$\mathrm{Re} = \frac{\rho_a v_{rel} d_h}{\mu_a}, \text{ where the hydraulic diameter } d_h = \frac{4(L_{g,w} \cdot L_{g,h})}{2(L_{g,w} + L_{g,h})} \quad \{3\}$$

The relative velocity for air is defined as $v_{rel} = v_a - v_x$, where v_a is the air velocity in the groove and v_x is the wall velocity.

Theoretical Minor Losses in Air Flow

The aerodynamic properties of the grooved roll at the closing and opening nips depend on the groove geometry, roll radius and surface velocity. At the air flow entrance and exit, losses can be measured from the 3D simulation model. The air flow path number 2 in

Figure 13 depends on the minor losses.

The grooved roll parameters: the groove filling angle α_f at filling point, area weighted average pressure at wall $\overline{p}_{wall}$ (double dash dotted line) and near the groove top $\overline{p}_g$ (dash dotted line) shown in Figure 14. The groove filling angle α_f is measured from 3D model from the groove top at radius r, where radial velocity $v_{rad} < 0$ on the closing nip side and on the opening nip side $v_{rad} > 0$. The groove filling angle is counterclockwise positive starting from the tangent point. The opening nip side pressures are defined in similar manner. The subscript for the closing nip side is *f,* and for the opening nip side the subscript is *e*.

The area for affecting pressure is obtained on the basis of the filling angle at the groove top and wall surface. The curve length of the groove top affecting the pressure area denoted with $\overline{p}_g$ is used at the wall surface as length of $\overline{p}_{wall}$. The average radial velocity $\overline{v}_{rad}$ and average wall velocity component $\overline{v}_1$ at angle β are measured from the 3D model.

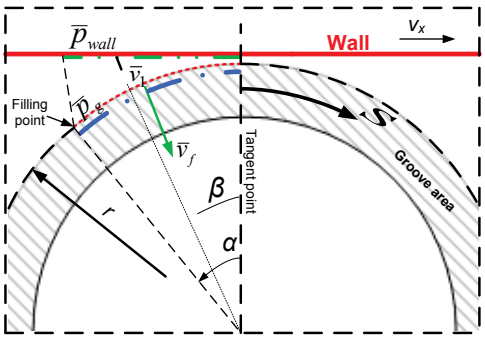

Figure 14 – The groove filling area with nomenclature.

Since the flow experiences friction and minor losses, the Bernoulli equation is not valid. Adding the minor loss coefficient K and assuming $\bar{v}_1 = v_x \sin\beta$, the equation is now

$$\bar{p}_{wall} + \frac{1}{2}\rho_a(\bar{v}_1)^2 + \rho_a g z_1 = \bar{p}_g + \frac{1}{2}\rho_a(\bar{v}_{rad})^2 - K\frac{1}{2}\rho_a(\bar{v}_{rad})^2 + \rho_a g z_2 , \qquad \{4\}$$

where $z_1 = z_2$.

The minor loss coefficient K can be solved from Equation {5}

$$K = 1 - \left[\frac{2(\bar{p}_{wall} - \bar{p}_g) + \bar{v}_1^2}{\frac{\rho_a}{\bar{v}_{rad}^2}} \right] \qquad \{5\}$$

In the numerical model the area weighted average of the radial velocity $\bar{v}_1$ at the surface of the wall can be used as well.

2D Simulation Tool: "Porous Media Approach"

The purpose for the 2D simulation model is to be able to simulate 3D grooved roll effects. In the 2D model, the groove height, width, friction and minor losses are modeled with porous media and porous jump boundary conditions. The groove cross-sectional area is converted to a 2D model with effective groove height L_{eff}. Rice [6] has used a similar method for effective groove height. This way the groove cross-sectional area and volume flow through the groove is the same with both 3D and 2D models. For a rectangular shaped groove the effective groove height L_{eff} is

$$L_{eff} = \frac{L_{g,w} \cdot L_{g,h}}{L_{g,w} + L_{l,w}} \qquad \{6\}$$

In Figure 15, the modification from the 3D groove to 2D effective groove height is presented.

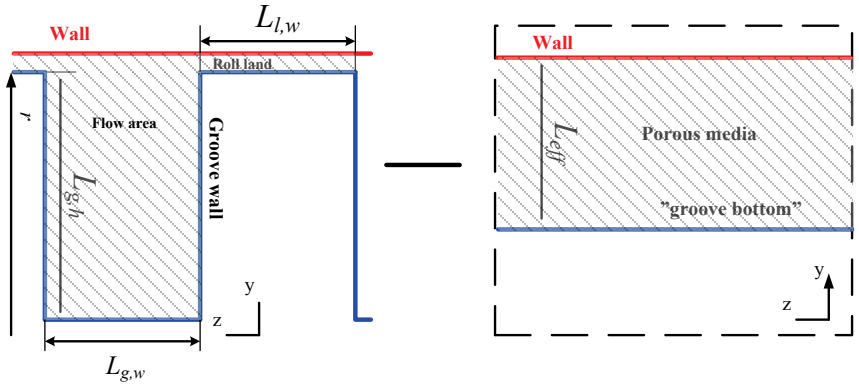

Figure 15 – The effective groove height with nomenclature.

The 2D model describes the groove wall friction and minor losses with the help of porous media and porous jump boundary conditions. The groove wall friction effects are calculated with the equations of viscous fluid flow inside ducts. The surfaces are assumed to be hydraulically smooth.

$$\frac{dp}{ds} = \frac{f}{d_h}\frac{\rho_a v_{rel}^2}{2}, \qquad \{7\}$$

where f is friction factor. The friction factor depends on the Reynolds number and it is shown in Equation {8} [8].

$$\begin{cases} f_{lam} = \dfrac{64}{\mathrm{Re}} & \mathrm{Re} < 2300 \\ f_{turb} = 0.316\,\mathrm{Re}^{-1/4} & 4000 < \mathrm{Re} < 10^5 \end{cases} \qquad \{8\}$$

The grooved area friction source term S_i is obtained with 2nd degree polynomial curve fit by combining Equations {7} and {8}. The source term S_i is

$$S_i = -(D v_i + C v_i^2), \qquad \{9\}$$

where D is the viscous loss term and C is the inertia loss term [1]. The minor loss K explained above is modeled in 2D by using the porous jump boundary condition

$$\Delta p = -\left(\frac{\mu_a}{\alpha} v_{rad} + K_{2D,\exp}\frac{1}{2}\rho_a v_{rad}^2\right)\Delta m, \qquad \{10\}$$

where α is permeability of the medium, K_{2D} the pressure-jump coefficient, and Δm is the thickness of the medium [1]. The 2D model is not able to capture the flow area change in the roll axial direction and a new measure has to be considered. Based on the groove and roll land width, the dimensionless measure groove fraction G_f is defined as in Equation {11}

$$G_f = \frac{L_{g,w}}{L_{g,w} + L_{l,w}} \qquad \{11\}$$

The minor loss calculated with the help of the 3D model has to be modified. Based on the continuity, the minor loss K_{2D} is

$$K_{2D} = \frac{K}{G_f^2} \qquad \{12\}$$

The 2D grooved roll model with the boundary conditions is shown in Figure 16.

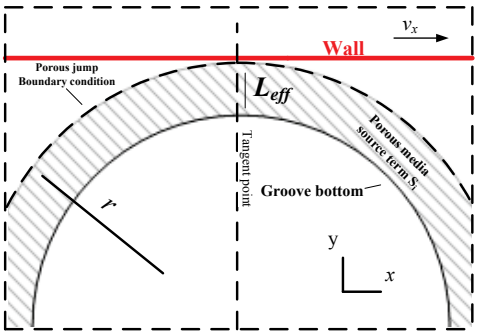

Figure 16 – 2D grooved roll model with boundary conditions and nomenclature.

RESULTS

In the following, CFD simulation results of a 3D and 2D grooved roll interacting with a moving horizontal wall are presented. The simulations are based on Reynolds averaged Navier-Stokes equations performed with a commercial CFD-code called ANSYS Fluent. The turbulence model is an RNG *k-e* model with a two-layer zonal model. Details for the governing equations and the used turbulence model can be found in [1, 4]. In both CFD models, air is treated as ideal gas. The system is assumed adiabatic, where the temperature is T = 300K. The roll and wall surfaces are assumed to be hydraulically smooth. The volume flows through the 2D grooves are adjusted with the porous jump boundary condition to be the same as with the 3D models.

The pressure curves have been plotted from the horizontal wall surface as a mean value to the *z*-coordinate. In other words, the effect of roll land and groove can be seen at tangent point. The tangent point of the model is in location x = 0 or α = 0. The closing nip is located at x < 0 and opening nip at x > 0. The flow development length (L = 3m) is constant in all the 2D and 3D grooved roll models. In the following, changes in surface velocities, groove width and groove height as well as the roll radius are presented.

The filling of the groove is measured from the top of the groove. The groove filling point is where $v_{rad,f} = 0$ and the filling angle is α_f. Similarly, the emptying point is at $v_{rad,e} = 0$, and the emptying angle is α_e. In order to compare the radial velocities between 2D and 3D models, the 2D radial velocity needs to be modified as shown in Equation {13}.

$$v_{rad}^{*} = \frac{v_{rad,2D}}{G_f} \qquad \{13\}$$

In Figure 17, the radial velocity at the groove top as a function of the roll angle α is presented with nomenclature. A comparison of the radial velocity curves in 2D and 3D models is shown as an example. The 3D model is marked with the continuous line and 2D with the dash-dotted line. The used geometry is the reference point where the roll radius is R. As a result, the 2D model seems to give almost the same radial velocity curve as the 3D model.

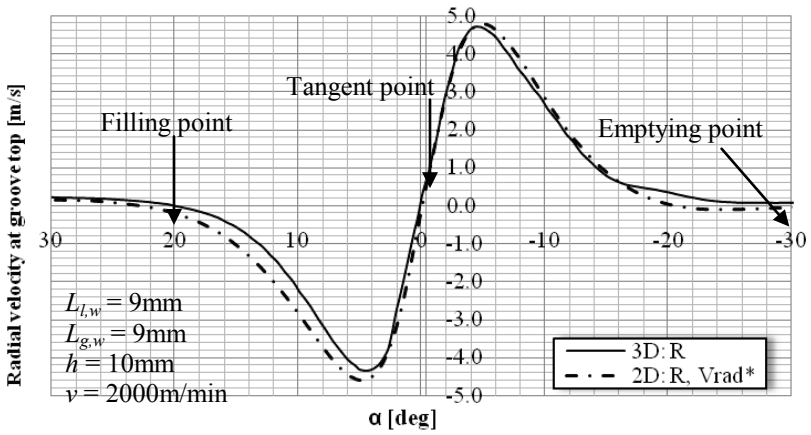

Figure 17 – Radial velocity at the closing and opening nips with the 2D and 3D models.

For each model, some characteristic values can be used to evaluate the groove performance and functionality. In Table 3, filling fraction V_f and angle α_f, as well as the groove minor loss K are shown for the 2D and 3D models. The rows present changes to roll geometries to see the changes in roll performance. The first row is the reference geometry. The roll properties which are changed are shown in the first column as underlined and bolded.

A comparison of the 2D and 3D models reveals that the filling angle behaves rather linearly, overestimating systematically 3 degrees with the 2D model. The filling fraction and minor losses show that the friction closing nip area between the roll land and wall has a greater effect than assumed. When the roll radius is doubled, the 2D model needs a significantly greater minor loss coefficient in order to maintain the desired volume flow through the groove. It needs to be reminded that the used source term S_i is based on an assumption of groove friction shown in Equations {7-9}, which affects to the flow parameters as well.

R-$L_{g,w}$-$L_{l,w}$-$L_{g,h}$-$L_{g,w}$-v	$V_{f,3D}$ [-]	$V_{f,2D}$ [-]	$\alpha_{f,3D}$ [°]	$\alpha_{f,2D}$ [°]	K [-]	$K_{2D,exp}$ [-]
R-9-9-10-2000	0.460	0.694	20.4	23.1	11.3	24.4
R-9-9-10-***1000***	0.625	0.692	18.9	22.3	11.7	25.3
R -9-9-***20***-2000	0.563	0.685	26.7	32.4	15.0	8.8
2R-9-9-10-2000	0.308	0.705	13.8	17.0	5.5	43.5
R -***3***-9-10-2000	0.474	0.591	11.4	14.5	9.7	12.7
R -9-***3***-10-2000	0.639	0.707	25.2	29.2	21.7	4.2

Table 3 – Aerodynamic properties of selected 2D and 3D grooved roll models.

In Figure 18, the surface velocities are varied. Static pressure is plotted as a function of the x-coordinate. The roll radius is R. Static pressure decreases at the tangent point when the dynamic pressure increases. The air flow is turbulent at the tangent point inside the groove. The Reynolds number Re varies between (1000 - 2000 m/min) 5000 => 11700.

A comparison between the 2D and 3D models reveals that at the closing nip side x < -0.02 and opening nip side x > 0.02m, the pressure curves are identical. The maximum pressure on the closing nip side is around 50 Pa for 2000 m/min for 2D and 3D models, which is not desirable for paper machine environments. The minimum pressure is just after the tangent point, at the opening nip side with the 3D model. The highest underpressure locates at the tangent point with the 2D model. Variations in the pressure curves at -0.02 < x < 0.02 m are related to friction and minor losses with the 3D model, where the wall is very close to the roll land. At the tangent point, the 2D grooved roll model underestimates the underpressure. The 2D grooved roll model uses the averaged approach because of the porous media boundary conditions, and therefore small variations in the curves cannot be seen.

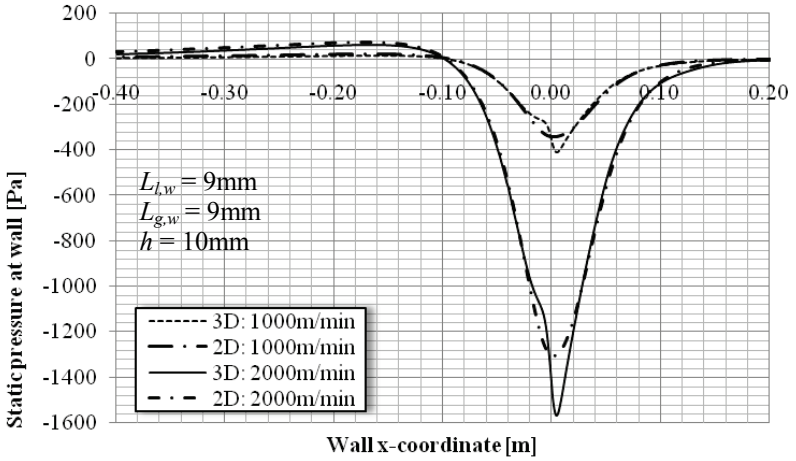

Figure 18 – Effect of velocity v_x to pressure distribution with the 2D and 3D models.

Groove height adjustment increases the cross-sectional flow area in the grooves. This helps the boundary layer flows to fit into the grooves with lower pressure in the closing nip area. A roll with deeper grooves now has higher ability to move the air between the closing and opening nip. A comparison with the smooth roll reveals a tremendous difference in the pressure development. A comparison between a smooth and grooved roll can be found in [5]. The 2D model differs slightly from the 3D model at the closing and opening nip sides, and thus the difference is in a good agreement. In Figure 19, the pressure distribution for the groove height of 20mm is presented with the 2D and 3D models.

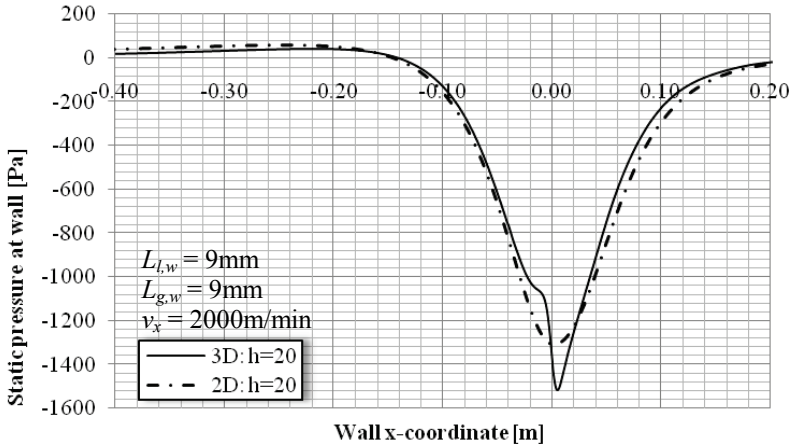

Figure 19 – Effect of groove height to the pressure distribution; a comparison between 2D and 3D models.

The roll radius influences the pressure distribution. A larger roll radius results in a wider underpressure area. From the web handling point of view, a wide underpressure area could be desirable. The 2D model overestimates the closing nip overpressure by about 50 Pa. At the tangent point the 3D model predicts a slightly higher underpressure. Figure 20 shows the pressure distribution with roll radius 2*R*. The 2D and 3D models are compared.

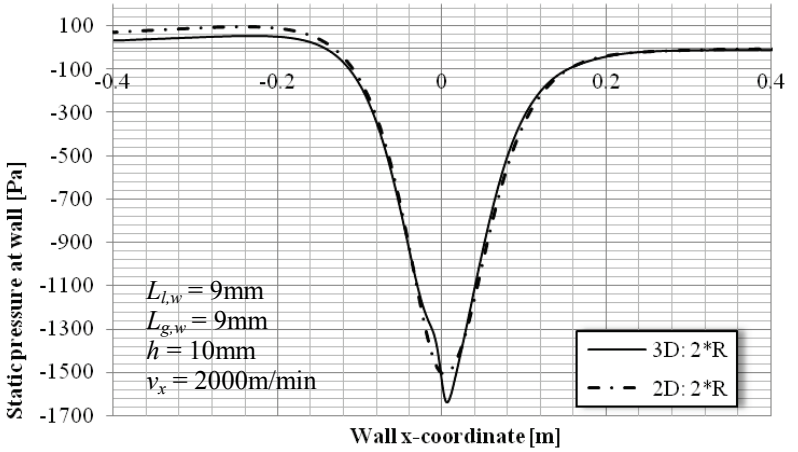

Figure 20 – Effect of roll radius on the pressure distribution with 2D and 3D models.

Variations of groove width $L_{g,w}$ and roll land $L_{l,w}$, when the groove height $L_{g,h}$ and surface velocity are kept constant gives more information about the pressure distribution at the wall surface in the vicinity of the closing and opening nips.

A wide groove compared to roll land width gives beneficial results for the pressure distribution. The closing nip overpressure is lower without losing much of the underpressure at the tangent point. When the roll land is wide, the friction and minor losses at the nip areas increase, which affects the underpressure distribution. The

narrower groove with the 2D model gives a better estimation on the location of the highest under pressure peak. When the groove land is narrow compared to the groove width, the 2D model gives very accurate prediction for the pressure at the wall surface. Only small overestimation in the closing nip pressure can be observed. In Figure 21 and Figure 22, the groove width and roll land measures are modified, and the results are compared between 2D and 3D models.

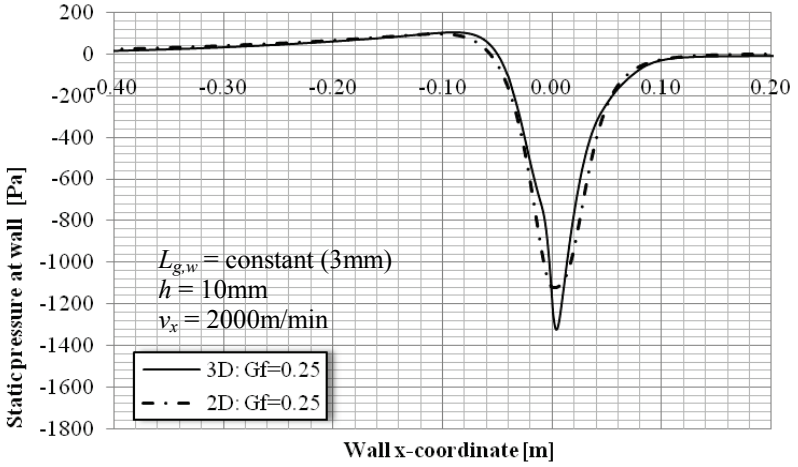

Figure 21 – Variation of roll land with the 2D and 3D models.

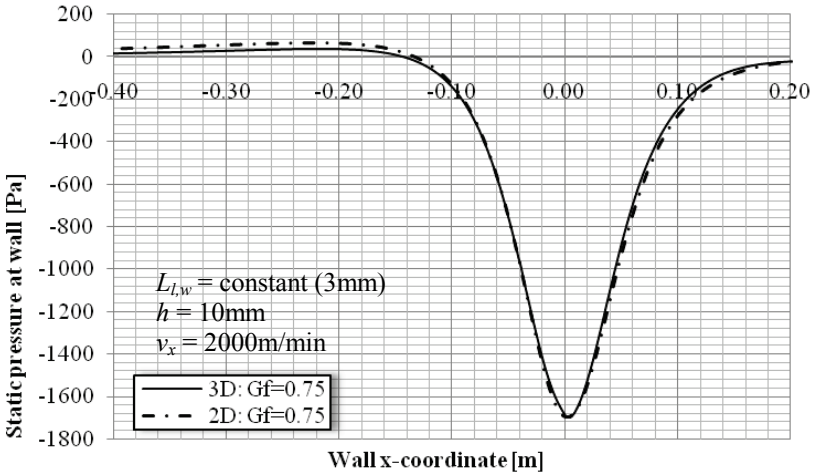

Figure 22 – Variation of groove width with the 2D and 3D models.

The presented results are based on computational fluid dynamics. Calculation mesh refinements have been performed in order to see if the mesh is dense enough. The refinement has been done with a grid adaptation tool based on y^+ values suggested for a *k-e* turbulence model with enhanced wall functions [1].

CONCLUSIONS

The complexity of solving the governing Navier-Stokes equations and the sheer variability of paper machine constructions makes a comprehensive *analytical* study of the roll-grooving effect difficult. One result of the present study is that the topology of the roll surfaces can have a tremendous impact on the overall runnability potential of the paper web. In order to minimize the overpressure peak at the closing nip, the groove fraction G_f should be as large as possible. The groove height $L_{g,h}$ has an impact on the pressure loss and the ability of the grooves to move air between the opening and the closing nip. Therefore groove size optimization has to be done on the basis of web handling device geometry, velocity of surfaces, and the needed underpressure.

The pressure curves simulated with the proposed 2D simulation tool were in good agreement with 3D simulation results in the closing and opening nips. Investigation of the characteristic aerodynamic properties of the groove such as the groove filling fraction and angle revealed differences between the 3D and 2D models. Therefore a further study of the air flow behavior with larger coverage angle is needed in order to find important factors for modeling the grooved rolls. The simulations were performed with a grooved roll model where the roll interacted with the moving horizontal wall where the coverage angle was differentially small. In this type of a model, the minor losses dominate and the role of the groove friction losses are not clear. In the 2D model, groove friction source terms for the porous media were calculated according to the pipe flow theory. Minor losses were described with the porous jump boundary condition with the assumption of equal volume flow through the grooves of the 2D and 3D models. The minor loss coefficient calculated by Equation 5 differed from the 2D values, which were obtained experimentally.

As a solution strategy, first 3D model with a chosen groove geometry needs to be created, to obtain the volume flow through the groove. The second step is to create a 2D model where the friction source term is obtained from the pipe flow theory. The third step is to adjust the porous jump boundary condition so that the volume flow through the groove is equal to the 3D model. At this point the parameters for the 2D model are ready to be used in more complex grooved roll geometry including other web handling devices.

From the simulation point of view, the limitations of computer and modeling resources cause the fact that simulations at paper machine scale with grooved rolls are not possible without the suggested simplifications. Validations of the models with appropriate measurements are a necessity, and will be performed in the future.

ACKNOWLEDGMENTS

The authors would like to thank Albany International, the Finnish Funding Agency for Technology and Innovation (TEKES), Metso Paper, and Process Flow Ltd Oy for supporting the research. Special thanks to Professor Jari Backman at Lappeenranta University of Technology for reviewing the paper.

REFERENCES

1. Fluent Inc., Fluent 6.3 User's Manual, 2006.
2. Karlsson, M., ed., Papermaking Science and Technology 9, Papermaking, Part 2, Drying, Fapet Oy, Helsinki, 2000.
3. Kurki, M. and Martikainen, P., "Adaptive, Self-Underpressurizing Suction Roll for Fast Web Handling," Proceedings of the Eight International Conference on Web Handling (IWEB 2005), Stillwater, Oklahoma, 2005.

4. Laakkonen, K., "Method to Model Dryer Fabrics in Paper Machine Scale Using Small-Scale Simulations and Porous Media Model," International Journal of Heat and Fluid Flow, Vol. 24, 2003, pp. 114-121.
5. Nurmi, S., Bergström, F., Immonen, E., Lehtinen, A., Juppi, K., and Martinsson, L., "Comparison of Aerodynamics Between a Smooth and Grooved Roll Interacting with a Rigid Impermeable Horizontal Wall," Proceedings of Paper Making Research Symposium (PRS 2009), Kuopio, Finland, 2009.
6. Rice, B. and Gans, R., "A Simple Model to Predict Web-to-Roller Traction," Proceedings of the Seventh International Conference on Web Handling (IWEB 2003), Stillwater, Oklahom, 2005.
7. Sasaki, M., Tanimoto, K., Kohno, K., Takahashi, S., Kometani, H., and Hashimoto, H., "In-Roll Stress Analysis Considering Air-Entrainment at the Roll-Inlet with the Effect of Grooves on Nip Roll Surface," Journal of Advanced Mechanical Design, Systems, and Manufacturing, Vol. 2(1), 2008, pp. 133-145.
8. White, F. M., Fluid Mechanics, 4th ed., McGraw-Hill, Boston, 1999, pp.175-176.

Modeling Grooved Rolls with Moving 2D Porous Media	**S. Nurmi[1], F. Berström[1], E. Immonen[1], A. Lehtinen[1], K. Juppi[2], and L. Martinsson[3],** [1]Process Flow Ltd Oy, FINLAND, [2] Metso Paper Oy, FINLAND, and [3]Albany International AB, SWEDEN

Name & Affiliation	**Question**
Dilwyn Jones, Emral Ltd.	Is there any reason why you chose a solid wall which is flat and moving to model a flexible paper moving over a grooved, rotating roll?
Name & Affiliation	**Answer**
Simo Nurmi, Process Flow Ltd. Oy	We often begin research with simple models and then increase the complexity later after it is determined what factors are most important in simulating reality. I know that the wall must be flexible and permeable to achieve realistic results. We have developed tools for that which I will show tomorrow.

DISCUSSION I

Leaders: **B. Kandadai**, Kimberly-Clark Corporation, and **J. K. Good**, Oklahoma State University, USA

Name & Affiliation	**Comment**
J. K. Good, Oklahoma State University	Let us consider what we have heard discussed today. First there was much work presented on various kinds of roll modeling. First we heard how nip mechanics develops wound-on-tension in winding rolls. We heard about use of models to prevent defects and we heard about gentle wavy defects. We heard about the latest axisymmetric models and we heard about nonlinear models. This afternoon, we heard two papers presented that were not specific to winding but had application to winding. We now have the opportunity to have an interactive discussion where people ask questions and hopefully get answers from either the authors or from other people in the audience. There were instances today where the time allowed for questions and answers was inadequate. We hope that if you had questions then that went unanswered during those periods that you will now take the opportunity to present them.
Name & Affiliation	**Question**
Steve Lange, Procter & Gamble	I have a question about the axisymmetric winding code. What do you think that code could tell us about wrinkle tendencies in a roll that has varied thickness across the width?
Name & Affiliation	**Answer**
J. K. Good, Oklahoma State University	Axisymmetric models allow us to study compressive stresses that could form in the axial or tangential direction in the wound roll. These models can be used to study how these stresses vary as a result of thickness nonuniformity. Thus these models can help us predict local buckling within wound rolls. These models also help us predict the shape of the wound roll during the winding process. We know that roller shape can induce wrinkles in webs, tapered rollers and convex rollers for instance. If the web thickness nonuniformity was to produce a wound roll that was convex in shape, wrinkles could be produced when the roll shape acquired a critical level of convexity.
Name & Affiliation	**Question**
Tim Walker, T J Walker & Associates	This question regards the axisymmetric roll modeling too. It appears that next generations of winding defects that can be studied are internal bucking defects within wound rolls. Most of the web instabilities that have been studied to date are those that involve a web in a free span. Are we now moving to studying the buckling of curved webs or laminates in a wound roll where that web may be stabilized by surrounding layers under pressure?
Name & Affiliation	**Answer**
J. K. Good, Oklahoma	This is correct. As models develop we gain the capacity to

State University	treat defects of higher complexity. The stars we saw in Dr. Hashimoto's rolls this morning could have been the result of a core relaxing through time since fiber cores are viscoelastic structures. As the winding models progress we may move from an elastic core model to a viscoelastic core model. So models progress and as they progress they allow us to study new defects. The defect may not be new but our ability to study the defect is. You may have noted large axial stresses in the core in the results of the axisymmetric model. For years it has been known the radial stiffness of cores is important in determining the radial and tangential stresses in the web wound near the core. Now it appears the axial stiffness of the core is also important. You might go so far as to say this is unfortunate since the axial and radial stiffness of fiber cores is rarely known well. But knowledge of these properties and their relaxation may be critical to prevent web defects that are common in the vicinity of a core. Axisymmetric winding models allow us to study the compressive stresses which must be present for internal buckling within wound rolls to exist. Now the defect models must improve because buckling of web layers within the wound roll is more complex than buckling of webs in free spans.
Name & Affiliation	**Question**
Dilwyn Jones, Emral Ltd.	I have a question for Bob Bettendorf concerning the intelligent roll. Are there any specific roll dimensions that need to be satisfied for use of that system? Is this transportable from small all the way to big rolls?
Name & Affiliation	**Answer**
Bob Bettendorf, Metso Paper, USA	The only real limitations are (1) 100 mm between the end of the roll and the bearing housing and (2) a roller diameter that is greater than 400 millimeters.
Name & Affiliation	**Question**
Michael Desch, Technical University of Darmstadt	This question also pertains to the intelligent roll system. If I understood you correctly the principle for measuring the stresses can be affected by the deformations of the roller. When the intelligent roll is used as a nip roller, do you apply more force to the nip roller to compensate for the increase in the area of contact to control the contact pressure?
Name & Affiliation	**Answer**
Bob Bettendorf, Metso Paper, USA	We choose to cover rollers with stiffness in mind so that we don't end up with a situation where our sensor deflects more than the surrounding area. We take this into account so that we don't have excessive deflection in the area of the sensor.
Name & Affiliation	**Question**
J. K. Good, Oklahoma State University	Do you carefully choose where you put these sensors and try to make sure the idlers or the nips have such a huge bending stiffness that you don't have to worry about their deformations?

Name & Affiliation	Answer
Bob Bettendorf, Metso Paper, USA	No, normally the pitch of the spiral is the more important consideration for locating these sensors on the roll. We haven't had to take into account the deformation of the reel drum.
Name & Affiliation	**Question**
J. K. Good, Oklahoma State University	Is this because there are other factors that force you to have high bending stiffness in those rolls to begin with so that bending deformation is not a problem?
Name & Affiliation	**Answer**
Bob Bettendorf, Metso Paper, USA	We design a reel drum to have adequate bending stiffness such that the first natural frequency is not excited at any operational speed. Such a drum is so stiff we don't normally worry about these things.
Name & Affiliation	**Question**
Dilwyn Jones, Emral Ltd.	This question pertains to the axisymmetric wound roll models. You talked about the axial strengths of cores. I was wondering in the axisymmetrical model, what do you do about the core? Is it restrained against expansion at the ends or do you allow it to expand outwards as the roll stresses go up?
Name & Affiliation	**Answer**
J. K. Good, Oklahoma State University	Different roll models do different things, but most do not constrain the core against axial expansion. That is something that is easy to change and you could simulate the stiffness of the core chuck. You could assume the core chuck stiffness is very high and is thus rigid. One of the benefits of finite element codes is that the primary unknown is displacements at nodes. This makes it easy for the user to assume various boundary conditions at the core ends such as rigid or perhaps elastic springs depending on the design and actuation of the core chuck.
Name & Affiliation	**Question**
Dilwyn Jones, Emral Ltd.	So the modeling you presented was with an unconstrained?
Name & Affiliation	**Answer**
J. K. Good, Oklahoma State University	The results presented were for very special cases. We were comparing to test data that was available publicly in the literature: Hakiel and Cole's Case A and Case B. Their core fixture was a set of aluminum rings that were instrumented with strain gages. These rings were free to expand in the radial and axial directions. In our model we assume the core to be continuous over the width of the roll. One end of the core is fixed to prevent rigid body motion in the axial direction. The opposite end is free to expand in these simulations. These boundary conditions are easy to change in the model and must be due to the multitude of core mandrel supports and chuck supports that exist. The good agreement shown between our results and that of Hakiel and Cole are an indication of how tiny the radial deformations of their core segments were.

Name & Affiliation	Question
Balaji Kandadai, Kimberly-Clark Corporation	Do we have the capability to analyze axial slip within a roll? Do axisymmetricwinding models have the capacity to show how axial deformations vary in a roll?
Name & Affiliation	**Answer**
J. K. Good, Oklahoma State University	Axisymmetric models have the capacity to report shear stresses in the rz plane and the pressure (normal forces) between web layers. With a know friction coefficient regions where slip will occur can be predicted. Axial deformation in the z direction is a direct output of axisymmetric finite element codes.
Name & Affiliation	**Question**
Dilwyn Jones, Emral Ltd.	Professor Hashimoto, this question pertains to winding core optimization. I was puzzled by your choice of optimization function. It seems that by minimizing the square of the deviations that you are trying to determine the critical values. Are you trying to reach the critical slippage each time or the critical wrinkling? It would appear you would want to operate sufficiently far from both the slippage and the wrinkling to operate in a safe regime. My experience with winding models is that if you have a large winding tension that will reduce the slippage. But if you also have a higher tension taper that will reduce the circumferential stresses and the tendency for wrinkling. This is because the circumferential stress will never become negative at any wound roll radius. It appears that you do not have the right optimization function yet. Perhaps another mathematical function might work better.
Name & Affiliation	**Answer**
Hiromu Hashimoto, Tokai University	High winding tension is usually used to avoid the slippage. I think too much high tension is not good. The optimization technique is very effective to avoid both slippage and static.
Name & Affiliation	**Question**
Jeff Forry, Adhesives Research	This question is with regard to the intelligent roll paper: What is your sampling rate on the encoder?
Name & Affiliation	**Answer**
Bob Bettendorf, Metso Paper, USA	I am not sure what the sampling rate is on the encoder. We have a method where we can use just a one pulse per revolution encoder or we can use a traditional pulse encoder. I am not sure what the number of pulses per revolution are on it. That part of the device is fairly proprietary.
Name & Affiliation	**Question**
Jeff Forry, Adhesives Research	I was trying to determine the resolution per differential segment.
Name & Affiliation	**Answer**
Bob Bettendorf, Metso Paper, USA	The actual spatial resolution of the sensor is about 50 mm across the width of the roll.
Name & Affiliation	**Question**
Robert Steves, Mitsubishi Polyester Film, Inc.	I have a question on the intelligent roller. I noticed on the picture of the roller that the sensors appear to be doubled in

	some areas but not in others. How do you isolate which sensor is responsible for the output?
Name & Affiliation	**Answer**
Bob Bettendorf, Metso Paper, USA	In Figure 14 we are showing two different spirals. If there were only one, it would be like you said. We would not be able to differentiate between the signals.